Scanning Microscopy

Volume 7 | Number 4 Article 5

12-31-1993

Imaging-SIMS (Secondary Ion Mass Spectroscopy) Studies of Advanced Materials

R. Levi-Setti
The University of Chicago

J. M. Chabala
The University of Chicago

J. Li
The University of Chicago

K. L. Gavrilov
The University of Chicago

R. Mogilevsky
The University of Chicago

See next page for additional authors

Imaging-SIMS (Secondary Ion Mass Spectroscopy) Studies of Advanced Materials

Authors

R. Levi-Setti, J. M. Chabala, J. Li, K. L. Gavrilov, R. Mogilevsky, and K. K. Soni

Scanning Microscopy, Vol. 7, No. 4, 1993 (Pages 1161-1172)
Scanning Microscopy International, Chicago (AMF O'Hare), IL 60666 USA

0891-7035/93$5.00+.00

IMAGING-SIMS (SECONDARY ION MASS SPECTROSCOPY) STUDIES OF ADVANCED MATERIALS

R. Levi-Setti*, J.M. Chabala, J. Li, K.L. Gavrilov, R. Mogilevsky, and K.K. Soni

Enrico Fermi Institute and Department of Physics
The University of Chicago, Chicago, IL 60637

(Received for publication September 1, 1993, and in revised form December 31, 1993)

Abstract

This article describes the application of scanning ion microprobe (SIM) microanalysis for the characterization of advanced engineered materials. In conjunction with secondary ion mass spectrometry (SIMS), scanning ion microprobes can image elemental distributions over surfaces with high lateral resolution (50-100 nm). With this technique, most elements, including isotopes, can be detected with good sensitivity. The principles and instrumentation associated with the SIM/SIMS technique are briefly described and ongoing developments are outlined. The analytical capabilities of the technique are illustrated by case studies of aluminum-lithium alloys, zinc oxide varistors, aluminum matrix composites, and photographic materials.

Key Words: Secondary ion mass spectrometry (SIMS), scanning ion microprobe, materials, microanalysis.

*Address for correspondence:
R. Levi-Setti
Enrico Fermi Institute
The University of Chicago
5640 S. Ellis Ave
Chicago, IL 60637-1433
Telephone number: (312) 702-7827
FAX number: (312) 702-5863

Introduction

Microstructural characterization of materials is usually performed by light optical microscopy or one of the electron microscopy techniques. With these tools, information can be gathered on physical properties such as precipitate size and distribution, grain size, porosity and crystallographic defect structure. Beyond these form-and-shape measurements, it is often necessary to determine the chemical nature of microstructures. Materials microanalysis (as opposed to simple characterization) can be performed with several techniques, each with certain strengths. These techniques include X-ray microanalysis in scanning and transmission electron microscopy, scanning Auger electron microscopy, and electron energy loss spectrometry. This article describes imaging secondary ion mass spectrometry (SIMS) with a scanning ion probe (SIM) as a means for microchemical characterization. Because SIMS is sensitive to mass, not atomic number, it can be used to measure the distribution of all elements and isotopes in a sample. In certain cases, parts per million (ppm) concentration sensitivity can be attained.

With SIMS (as for several imaging microanalysis techniques), analytical information is best represented in the form of two-dimensional concentration distribution images (compositional "maps"). These maps facilitate the correlation of chemical information with corresponding physical features of the microstructure such as grain boundaries and pores. Compositional mapping can be useful for the analysis of materials where little prior information is available, because every location in the image field is sampled without any bias: after acquiring survey mass spectra, unexpected and unusual spatial distributions are often discovered. In stigmatic direct imaging SIMS instruments (commercially available from Cameca), the best spatial resolution is $\sim 0.5\ \mu m$. For the second class of SIMS instruments, scanning ion microprobes, the resolution can approach 20-50 nm. Scanning ion microprobe systems are available from several vendors and offer submicrometer-sized primary beams of Ga^+, Cs^+, O^-, etc. for a variety of analysis tasks. The attainable chemical sensitivity varies among the different breeds of imaging SIMS instruments; there is an inevi-

table tradeoff between spatial resolution and sensitivity. We save additional comments about SIMS sensitivity for the final section (**Future Prospects**) of this review. A final type of SIMS instrument, broad beam non-imaging SIMS, commonly employed for the characterization of bulk materials, is notable because it provides excellent sensitivity ($\sim$ parts per billion for favorable elements).

As illustrations of the power of the imaging SIMS technique (scanning probe-based), we have chosen examples from several topics in advanced materials. Although SIMS is frequently used for the characterization of electronic materials, it does not yet play a prominent role in the study of metallic and ceramic materials. The following case studies are briefly described: alloys (Al-Li-Cu), electronic ceramics (ZnO varistors), metal-matrix composites, and photographic materials. As will be shown, imaging SIMS has a significant role to play in the characterization of materials and its routine use is highly advocated. Analyses were performed using the high-lateral-resolution scanning ion microprobe operated at The University of Chicago. A bibliography of topical papers describing results obtained with this instrument is compiled in **Appendix 1**.

Experimental

Instrumental details and operating practice for the University of Chicago scanning ion microprobe have been discussed in numerous reports (Levi-Setti *et al.*, 1988a,b, 1991). The instrument utilizes a finely focused Ga^+ beam (typically, 40 nm FWHM, $\sim$30 pA), extracted from a liquid metal ion source, to sputter atoms and molecules from the topmost monolayers of a solid or liquid. The ion bombardment is perpendicular to the sample. As this beam is raster-scanned over the specimen surface, the resulting secondary ions are energy- and mass-filtered to produce mass-resolved images of the analyzed area. The results summarized in this manuscript were obtained with an radio frequency (RF) quadrupole mass spectrometer. Topographic information can also be obtained, without mass discrimination, by constructing an image with the total, non-mass-resolved ion-induced secondary ion (ISI) signal. This non-mass-resolved signal is gathered by a detector that overlooks the sample at an angle, producing a shadowing effect. On the other hand, secondary ion extraction for SIMS is perpendicular to the sample surface, eliminating shadowing problems (but not all edge effects). A typical SIMS image is acquired from scans of 512 x 512 or 1024 x 1024 raster elements and is accumulated in $\sim$1-10 minutes. The storage, processing and analysis of the resulting maps are accomplished by an image processing system closely interfaced to the secondary ion detectors.

The materials specimens discussed here were prepared using standard metallographic/ceramographic polishing procedures. A thin layer of gold was sputter-deposited onto the specimens to prevent charging during analysis.

Examples of Applications

The following examples emphasize the value of correlating microstructure and SIMS-derived microchemistry to the full understanding of advanced materials.

Al-Li-Cu alloys

Aluminum-lithium based alloys are being developed and used as replacements for other Al-based alloys in aerospace structural applications: the addition of Li bestows a fortunate combination of reduced density and increased elastic modulus. The microstructure of these alloys has been extensively investigated by transmission electron microscopy, although only a few studies have determined phase compositions and the alloy microchemistry (e.g., see references in Sanders and Starke, 1989). Knowledge of Li distribution in these alloys is critical to alloy development and to the evaluation of processing methods. This objective can be accomplished well by SIMS because of this technique's extremely high sensitivity for Li (ionization probability $\approx$ 1), in contrast to the practical insensitivity of other microanalytical techniques to this light element. With SIMS, a high signal-to-noise ratio for Li ($\sim 10^5$) implies that lateral resolution can approach the primary beam spot size (for scanning probes, $\sim$40 nm), permitting the detection of ultrafine detail in the Li distribution. (For all imaging analysis techniques, spatial resolution is inversely related to signal statistics.)

We have studied the distribution of Li in several Al-Li alloy systems with both a scanning ion microprobe and with direct-imaging SIMS instruments (Soni *et al.*, 1993a); an example is excerpted here which describes the chemical microstructure of an Al-Li-Cu alloy. A model Al-18.7 at.% Li-11.6 at.% Cu alloy was aged at 500°C for seven days in order to study the phase equilibria among the three principal ternary phases T_2 (Al_6Li_3Cu), T_1 (Al_2LiCu), and α (Al solid solution). To study the equilibria of these three phases, this model alloy was prepared with a high content of Li and Cu; commercial alloys are typically made with only 8-10 at.% Li and $\sim$1 at.% Cu. In commercial alloys, these ternary precipitates form thin platelets, $\sim$2 nm thick, and thus, defy detailed microchemical investigation.

Figures 1a and 1b (on color plate at page 1167) show the Li^+ (yellow) and Cu^+ (red) distribution maps superimposed on the corresponding Al^+ (blue) map. The individual maps have been coded in pseudocolor and superimposed in order to elucidate the spatial correlation of these elements. All maps were acquired from a polished surface of this ternary alloy, originating from the same $\alpha + T_1$ eutectic area. The analyses were performed in the absence of any oxygen on the specimen surface, which was precleaned with an intense Ar^+ beam within the vacuum of the instrument. In this image set, lithium and copper dominate in the T_1 phase; whereas, aluminum is concentrated in α, as expected. Unfortunately, the Cu^+ signal from this oxygen-free material is disproportionally small (this is a well-known SIMS chemical "matrix effect"). Nevertheless, it can be deter-

mined that T_1 is Cu-rich and that the Cu distribution is relatively inhomogeneous. This inhomogeneity can be understood in terms of the low diffusion rate for Cu relative to that of Al and Li. Trace amounts of O and F were detected in this specimen, and their distributions are displayed in Figures 2a and 2b; the presence of these elements was not known beforehand. These images were obtained from a similar eutectic region of the alloy and reveal complete sequestering of O and F to the T_1 plates. Oxygen is probably introduced by the oxidation of Li during casting. The near-ubiquitous fluorine contamination in Al alloys has been previously noted by our group and can be linked to the extraction of Al from cryolite (Na_3AlF_6).

Dopant distribution in ZnO varistors

ZnO varistors exhibit non-linear current-voltage (I-V) characteristics and are used in electronic devices such as surge protectors (Gupta, 1990). The properties of ZnO varistors are superior to those of SiC, its predecessor, and the market share of the former is continually rising. This material is produced by mixing semiconducting ZnO powder with powders of other metal oxides, e.g., Bi_2O_3, Sb_2O_3, CoO, MnO_2, NiO, Cr_2O_3, SiO_2, followed by conventional pressing and sintering. The ZnO varistor is a good example of "grain boundary engineered" materials: upon sintering, the additives are distributed in such a way as to render the grain boundaries more resistive than the grain interior. The most important component of this varistor is Bi_2O_3, which, because its solubility in ZnO is extremely small, forms a thin intergranular film and, depending on its volume fraction, some independent clusters. This Bi_2O_3 film is responsible for the highly resistive grain boundaries. The I-V non-linearity and the durability of ZnO varistor are enhanced by the addition of several other dopants (Gupta, 1990). A study of dopant distribution in commercial ZnO varistors with the University of Chicago SIM has been published (Soni *et al.*, 1992c). Here, we discuss the analysis of simple ZnO varistors, fabricated in-house, doped separately with Na and Li. The detection and mapping of Na and Li with imaging SIMS is quick and easy because of the intense secondary ion yields of these elements. It is extremely difficult or impossible to detect these elements using alternative analytical techniques; therefore, this case study exemplifies the pivotal role that imaging SIMS holds in materials characterization.

Sodium is also added to ZnO to improve varistor stability. A model explaining the action of Na was proposed by Gupta and Miller (1988). In brief, varistor degradation can be slowed down by reducing the concentration of Zn interstitials. Sodium occupies interstitial lattice sites, thus reducing the availability of such sites and also preventing the motion of Zn interstitials. These workers, using broad-area SIMS depth profiling, show that Na doping (accumulation) occurs in the grain boundary region. Figures 3a and 3b (on color plate at page 1167) contain superimposed, color coded maps of a polished section of a ZnO varistor sample that was doped

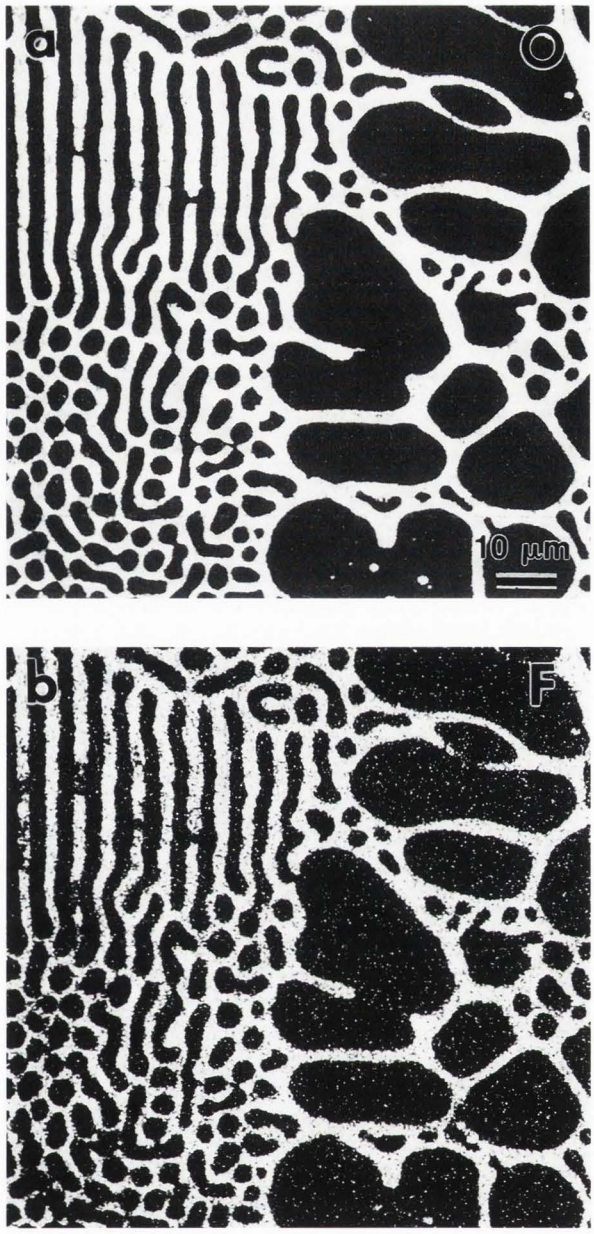

Figure 2. SIMS maps of an Al-Li-Cu alloy showing the distribution of (**a**) oxygen (as O^-) and (**b**) fluorine (F^-). The O and F distributions are similar to the Li distribution from this specimen area, suggesting complete segregation of these trace impurities to the T_1 phase.

---

only with Bi and Na. In Figure 3a, a thin intergranular layer of Bi_2O_3 is apparent (Bi is presented in red). The Na^+ map of the same area reveals that Na is largely segregated to the Bi-rich interface. We have assumed that the matrix effects for Na^+ SIMS emission are nearly the same for the ZnO and Bi_2O_3 phases. This assumption is reasonable, to first order, considering the high ionization probability of Na from most matrices. The presence

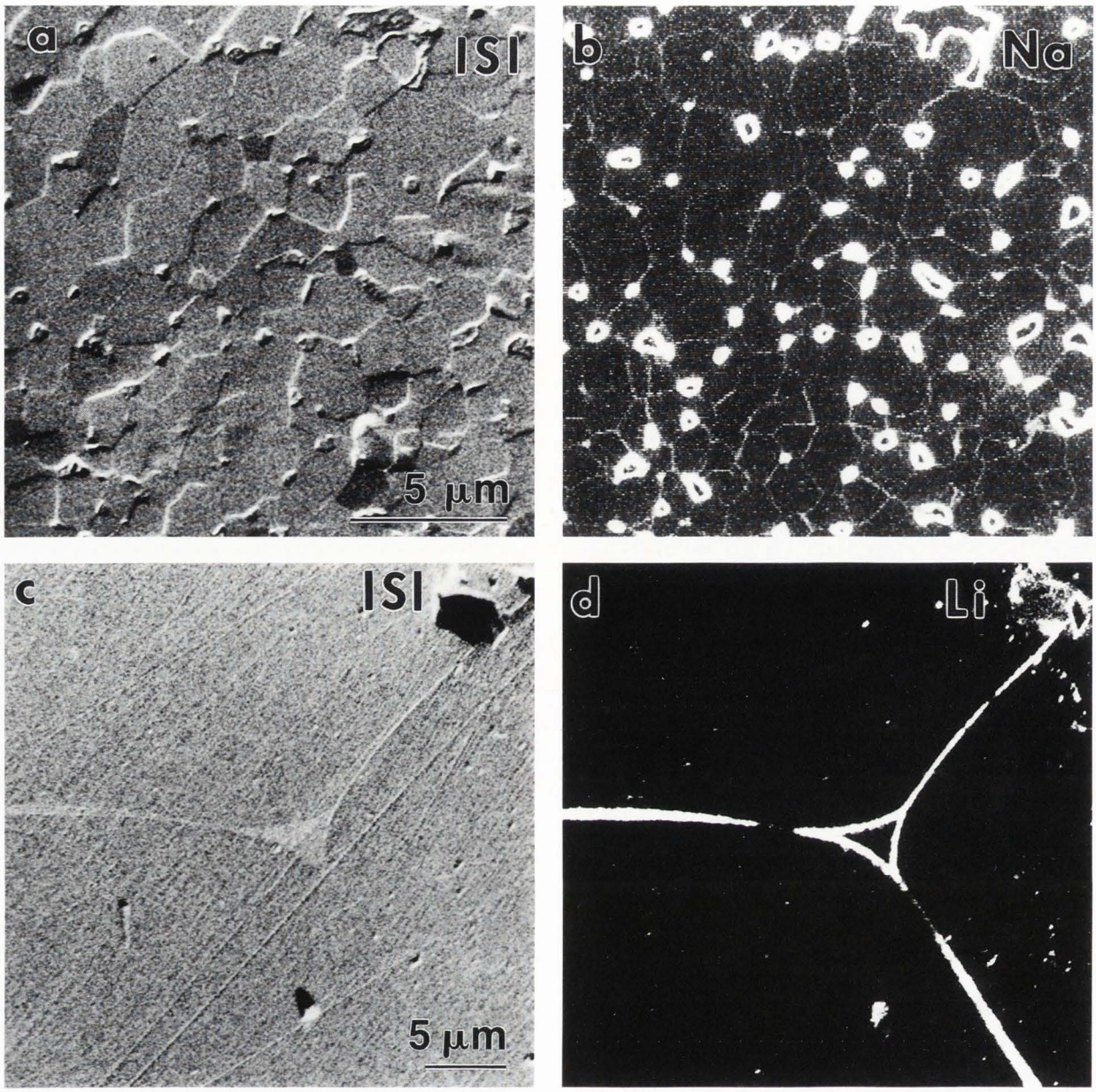

Figure 4. SIMS maps of ZnO doped with Na (**a**, **b**) and with Bi and Li (**c**, **d**). **a**. Ion-induced secondary ion (ISI) image displaying topographic contrast. **b**. Na^+ map. **c**. ISI image. **d**. Li^+ map.

of Na in the grain boundary layer may be a result of its high solubility in the Bi_2O_3 phase. These imaging SIMS observations substantiate the results of Gupta and Miller regarding Na distribution.

It is of interest to determine if grain boundary segregation of Na would occur in ZnO even in the absence of the Bi-rich grain boundary layer. Recall that Bi-doping is essential to create the varistor action in ZnO, which is semiconducting otherwise. Figures 4a and 4b show images of a ZnO sample that was doped only with Na, without any Bi. Figure 4a presents an ISI topographic map, showing the fine grain size of this sample. With the addition of Bi, the grain size increases, as demonstrated by a comparison of Figures 3 and 4. The Na^+ map clearly reveals segregation of Na to the ZnO grain boundaries (edge effects may be enhancing the Na contrast across some boundaries). Therefore, segregation of Na in ZnO does not require the presence of an intergranular Bi_2O_3 layer. Excess Na and impurities (mainly Si) combine to form second phase precipitates, approximately 0.3-1 μm in size.

Figure 4c is an ISI topographic image of a ZnO

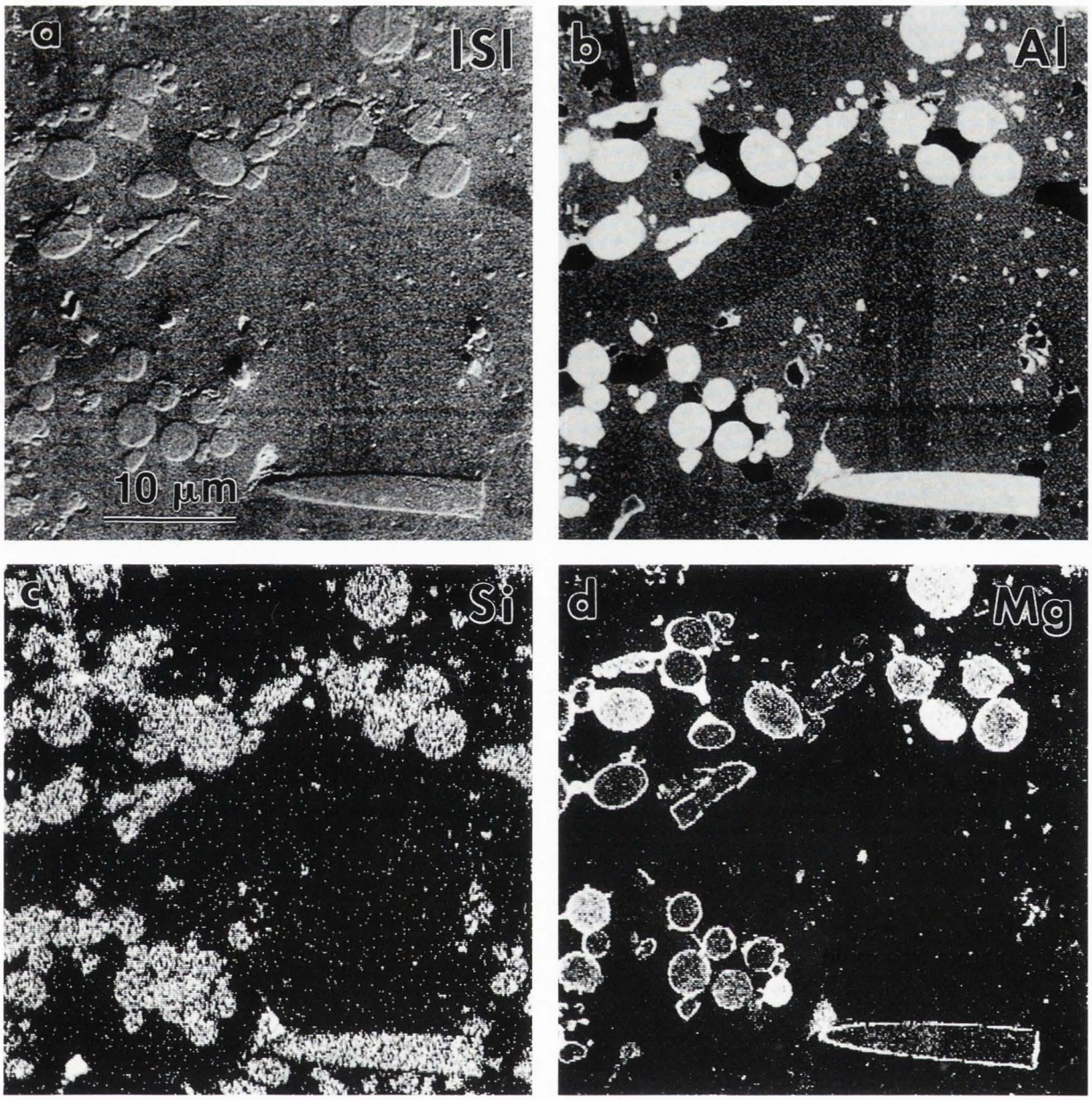

Figure 5. SIMS maps of a polished section of an Al-Si-Mg-Cu alloy reinforced with Saffil fibers. The composite was prepared by squeeze casting and subsequent T6 heat treatment (text). **a**. ISI image. **b**. Al^+. **c**. Si^+. **d**. Mg^+. The faint dark horizontal and vertical stripes are surface contamination.

sample doped with Bi and Li, displaying a grain boundary triple point near the center. The thin intergranular layer in this image is Bi_2O_3. Lithium addition enhances grain growth of the sintered ZnO product, which can influence the I-V characteristics of the material. The Li^+ map of the same area is shown in Figure 4d and reveals that Li is completely segregated to the intergranular layer. The Li^+ signal emitted from the ZnO grains is very small, suggesting that the solubility of Li in ZnO grains is negligible.

Metal-matrix composites

It is important to characterize interfacial phenomena in composite materials, because the interface plays a critical role in determining mechanical performance (e.g., see monographs by Dhingra and Fishman, 1986; Verpoest and Jones, 1991). Chemical interactions occur between the matrix and the reinforcing phase during fabrication and subsequent heat treatment. Among the chemical reactions occurring at the interface are oxidation, precipitation and interdiffusion. These reactions

are governed by the choice of the component materials, processing conditions, wetting/bonding agents, etc. Composites possess complex microstructures involving many light and minor elements distributed at the submicrometer level; the importance of high-spatial-resolution SIMS in the characterization of this rapidly growing class of materials is obvious. We have discussed benefits and limitations of the SIM/SIMS technique vis a vis composites in two reviews, which also included some examples (Soni *et al.*, 1993b; Williams *et al.*, 1993).

SIMS micrographs of an aluminum alloy reinforced with Saffil fibers are shown in Figures 5a-5d. The compositions of the constituents are as follows: alloy matrix: Al-9 wt.%, Si-1 wt.%, Mg-1 wt.%, Cu; and fibers: 96% Al_2O_3, 4% SiO_2. The composite was prepared by squeeze infiltration of a preform made of Saffil fibers coated with silica binder. Subsequently, the material was given a thermal treatment (T6) involving heating at 500°C for 6 hours followed by water-quenching. This treatment is usually administered to monolithic Al alloys in order to homogenize their composition, prior to low-temperature aging treatment which induces precipitation. We find that this treatment is not suited to this metal-fiber composite, because of intense reaction between the alloy and the reinforcement. The $^{28}Si^+$ signal is "contaminated" with a small amount of $^{28}AlH^+$: observations with a Si isotope indicate that the $^{28}Si^+$ map is qualitatively correct. The **Future Prospects** section of this paper describe attempts to improve mass resolution through the use of a magnetic sector mass spectrometer.

Figure 5a is a topographic image of a polished surface of this composite, showing mostly transverse cross-sections of fibers. The fibers appear as bright ovoids in the Al^+ map. The strong emission of Al^+ signal from the fibers is due to the presence of oxygen in this phase (which in general enhances the yields of positive secondary ions), despite the higher Al content in the Al-alloy matrix phase. Consequently, the fibers appear brighter than the Al-alloy matrix. Contrast interpretation in SIMS maps of composites, or of any material combining metal and ceramic phases, requires careful consideration of "matrix effects". The dark areas in the Al^+ map are bright in the Si map and, therefore, represent the free Si phase. The chemical interactions between the matrix and fibers are clearly manifested in the Mg^+ map: Mg from the alloy has reacted with the silica coating on the fiber and is also present within the fibers. Silica is reduced by both Mg and Al to form MgO and $MgAl_2O_4$ spinel. A comparison of the Al^+ and Mg^+ images indicates that the spinel phase replaces the silica coating around the fibers. Free Si, produced as a result of the reduction of silica, collects in large chunks in the vicinity of the fibers. The chemical interactions lead to a depletion of Mg from the alloy. Also, the binder is completely consumed and the fiber stiffness is lowered. A complete evaluation of this interesting material will be presented in future publications.

Legends for Figures 1, 3 and 6 on color plate
(on facing page).

Figure 1. Color-coded superpositions of SIMS maps of an Al-Li-Cu alloy. **a**. Al (blue) versus Li (yellow). The Li-rich area represent the eutectic T_1 (Al_2LiCu) phase. The Al-rich areas correspond to the solid solution α. **b**. Al^+ (blue) versus Cu^+ (red). The pink color is the result of Cu (red) coincident with Al (blue) in the T_1 areas.

Figure 3. Correlative color-coded SIMS map of a ZnO varistor doped with Bi and Na. **a**. Zn^+ (blue) and Bi^+ (red) distributions. **b**. Zn^+ (blue) and Na^+ (yellow). Na and Bi dominate in the intergranular layer.

Figure 6. Analysis of two silver bromide-based photoemulsions. **a**. Br^- (blue) and Cl^- (white) maps of hexagonal and triangular twinned tabular crystals. The Br distribution provides morphological information about the crystals. AgCl was grown epitaxially onto some of the vertices of the grains. **b**. Br^- (red) and I^- (white) maps of the top surface of cubic AgBr crystals with a surface monolayer of I. The iodine has been deposited preferentially along the border on each face of the cubes.

Photographic materials

Modern high-speed, high-resolution photography is possible because of advances in silver halide emulsion technology. Silver bromide crystals are naturally sensitive to blue light. To improve this native sensitivity and to expand it to other wavelengths, AgBr crystals are treated with sensitizers and are precipitated in various crystal habits, usually with the addition of iodine or other halides. The resulting engineered crystals are typically less than a micrometer in size. Additionally, they can have high aspect ratios, meaning they are much thinner ($< 0.1\ \mu m$) than they are wide. Photographic crystals are fragile, and can melt or curl under electron beam bombardment. Their small size implies that they are somewhat transparent to electrons, which can traverse the crystals without interaction.

Given the complexity (and commercial importance) of these engineered crystals, it is imperative that they be chemically characterized: the actual structure of the crystals must be compared to the predictions of the precipitation chemist and to the measured photographic efficiency. The analytical tools available for the study of these delicate materials are limited. Energy dispersive X-ray analysis (Gao *et al.*, 1989a; Chabala *et al.*, 1990) and backscattered electron studies (Gao *et al.*, 1989b, Geuens *et al.*, 1992a) of cryogenically cooled samples provide information about halide distributions. Atomic force microscopy (Keyes *et al.*, 1992) and low-temperature luminescence have also been directed toward this problem. A few researchers (for example, Maternaghan *et al.*, 1990; Geuens *et al.*, 1992b) have

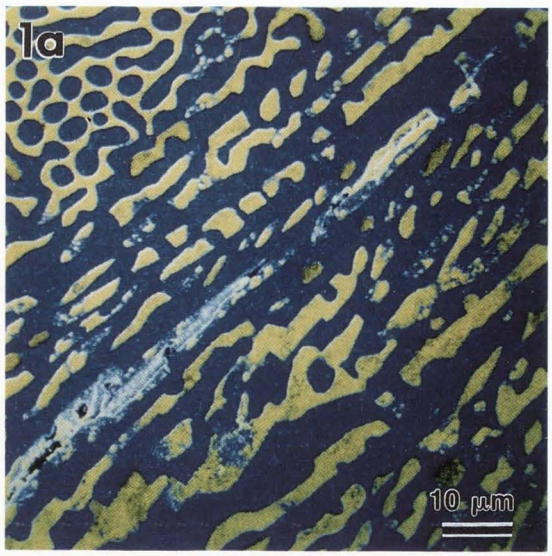
1a
10 μm

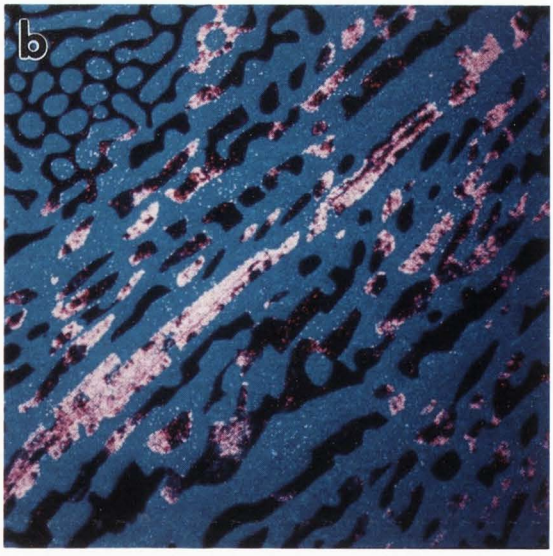
b

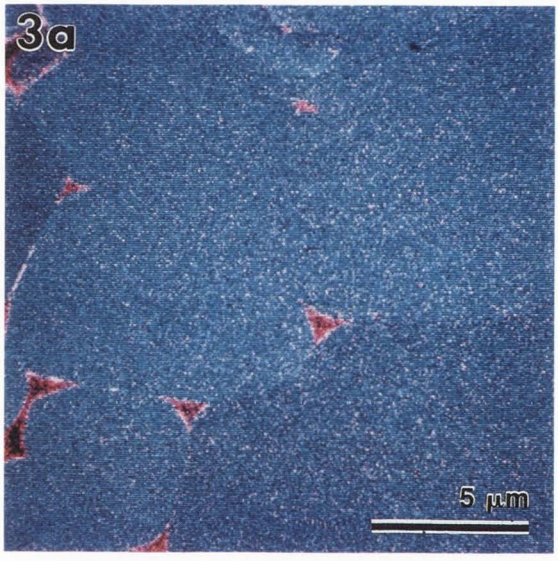
3a
5 μm

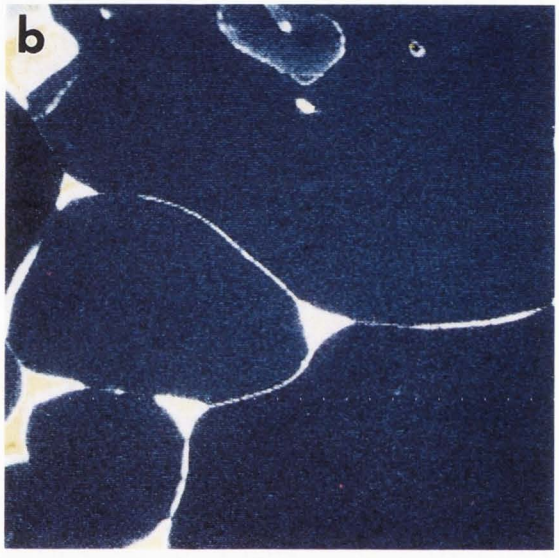
b

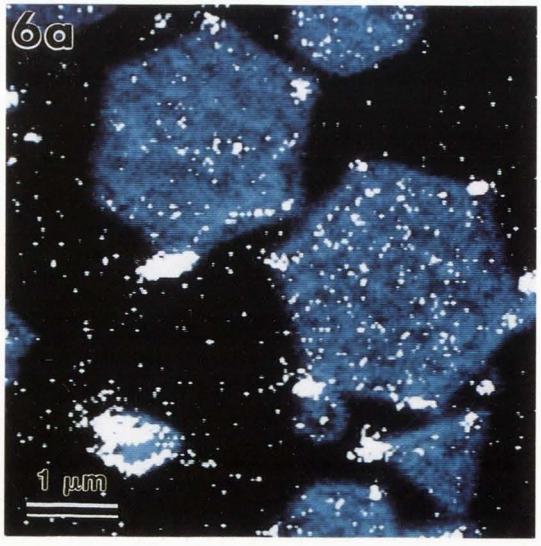
6a
1 μm

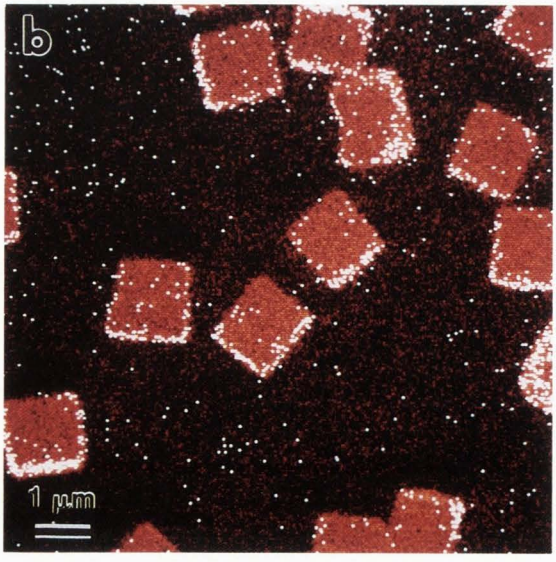
b
1 μm

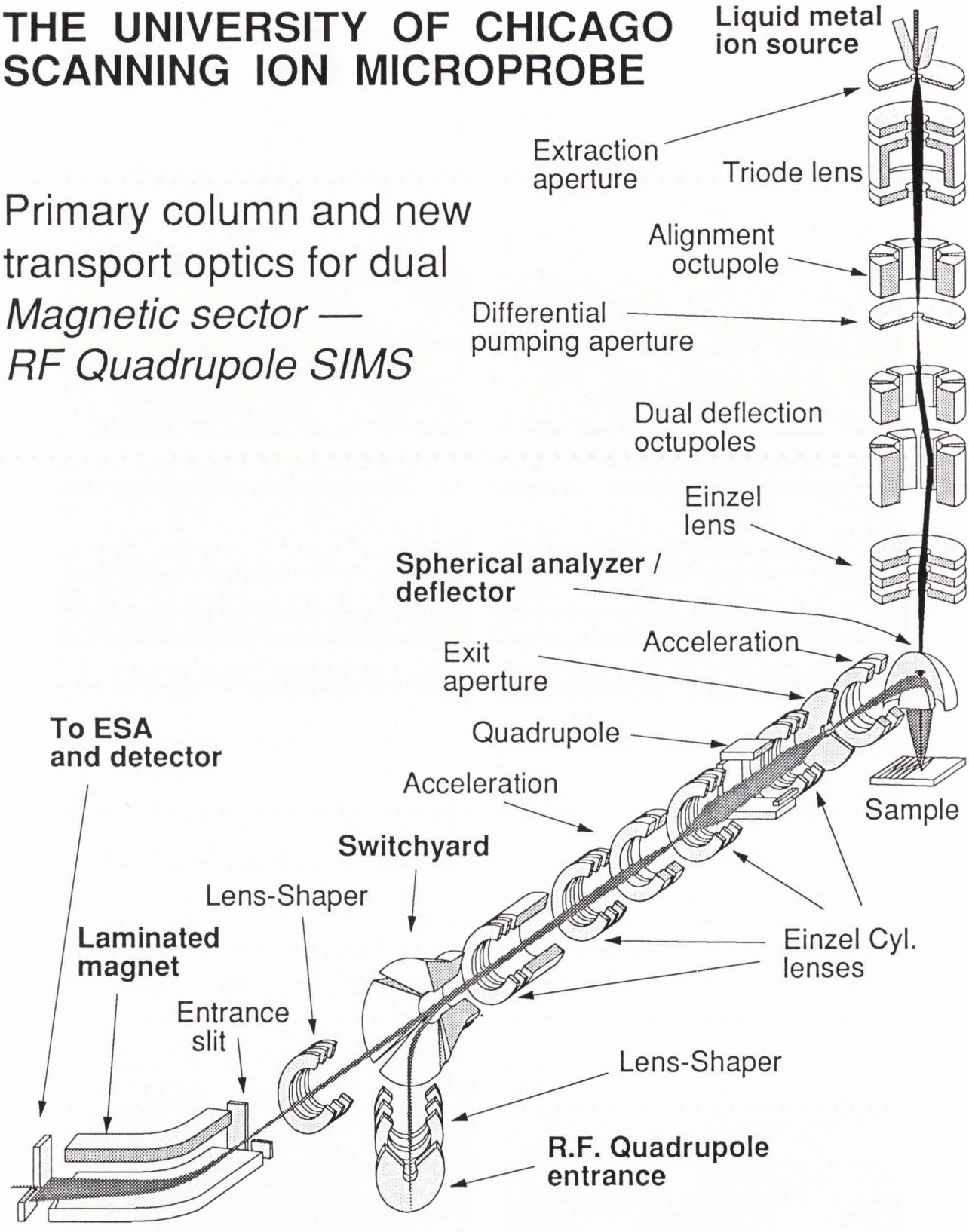

Figure 7. Schematic of the University of Chicago scanning ion microprobe with magnetic sector mass spectrometer. The primary ion system is the vertical assemblage at the right, the secondary ion system runs diagonally downwards to the left. Components not drawn to scale.

used secondary ion mass spectrometry to study silver halide crystals, with good reason: SIMS is very sensitive to the halide elements (because of their high electron affinity, the halides are emitted as negative secondary ions with almost 100% probability). As for electron beams, ion beams can damage photographic crystals. Care must be exercised when analyzing these crystals with SIMS, minimizing the primary ion dose. It is also desirable to cryogenically cool the sample, though in our experience this procedure does not improve the measurements. With SIMS, the primary beam affects, at most, a depth of 20 nm (with a 40 keV Ga^+ probe) below the surface of the crystals; whereas, with electron probe techniques, the crystals are bathed and penetrated with electrons, which can alter chemical distributions in these sensitive materials.

Two examples of SIMS analysis of these crystals are presented in Figure 6 (on the color plate at page 1167). Figure 6a shows two hexagonal and one triangular twinned tabular silver bromide crystals (Maternaghan *et al.*, 1990); the Br^- signal (blue) is used to record the overall structure of the crystals. The precipitation chemist has attempted to grow AgCl decorations on the corners of the crystals, as revealed by the white Cl^- signal. (These epitaxial decorations improve the photosensitivity of the material, perhaps by inducing lattice mismatch strain between the bulk crystal and the decorations.) Note that the chemist was not wholly successful: there is no Cl on the vertex at the upper left, near the **a**. Also, the site-direction of chloride was not complete, and some Cl specks are evident on the major faces of the crystals. To the best of our knowledge, these chemical measurements have not been achieved with other techniques.

Figure 6b shows a preparation of cubic monosize AgBr crystals. These crystals were prepared so that there is 13% of a monolayer of iodine on the surface (averaged over the surface), with no I in the bulk. This surface distribution was measured by rapidly scanning the probe once over a pristine area of the sample. The Br^- and I^- signals were measured simultaneously. By such means, the material is sampled over a depth < 6 nm, and atomic mixing is avoided. Clearly, the I is preferentially deposited on the periphery of the cube faces. This result is consistent with the hypothesis that I is adsorbed at crystal steps and terraces near the cube edges (Steiger *et al.*, 1991). Repeated measurements and analyses of several samples with varying I coverage assures that the I^- signal originates from the top surface of the cubes, not the edges (edge effect). It is worthwhile to reiterate that features less than 0.2 μm on these two photoemulsion materials are distinctly mapped by the scanning probe SIMS technique. As a tradeoff, the concentration of mapped constituents must be approximately 1% in order to be detected with adequate statistics at high spatial resolution with the University of Chicago scanning ion microprobe. We describe efforts to ameliorate this handicap in the next section.

Future Prospects

Researchers have learned to tolerate, if not be happy with, the quantification problems of SIMS. It is obvious that elemental sensitivity with SIMS is inversely related to spatial resolution, for the simple reason that higher resolution requires the removal of smaller microvolumes of material per image raster element. The literature on the quantification aspects of SIMS is endless; as a start, readers are referred to Benninghoven *et al.* (1987) and Chabala *et al.* (1988b). The RF quadrupole mass spectrometer, which has, until recently, operated on the University of Chicago scanning ion microprobe has functioned well as a tool for determining relative concentrations (parts per hundred) in submicrometer areas. To advance the performance of this instrument, the capabilities of the quadrupole mass filter have been supplemented by those of a magnetic sector mass spectrometer (Chabala *et al.*, 1992).

To combine high spatial resolution (< 0.5 μm) and part per thousand (or million) concentration sensitivity, magnetic sector, time-of-flight, and Fourier transform mass spectrometers can be used; there is not enough space here to properly discuss the advantages and disadvantages of each technique. Figure 7 shows in schematic form the recently-upgraded University of Chicago scanning ion microprobe. A spherical analyzer collector is positioned 1 mm above the sample surface. Secondary ions are accelerated into the collector by 200-300 V. This voltage, and the close sample-collector proximity, ensure that approximately 80% of the secondary ions enter the analyzer transport system (for ions with energy centered on the energy acceptance window). Significantly, the excellent primary ion focus and imaging of the instrument is not affected by this low-voltage collection strategy. In a unique design, the secondary ions are accelerated to full energy (5 keV) external to the primary optics and before the exit slit of the spherical analyzer. This structure greatly reduces the chromatic aberration of the secondary ion optics. The energy window of the system is 30 eV at full accelerating voltage and with open spectrometer slits. We have not fully explored operation with an energy offset (e.g., to separate mono-atomic from molecular interferences).

The secondary ions traverse a switch-yard deflector system, which has been fully modeled in three dimensions. Ions can be steered into the old RF quadrupole spectrometer, or can continue straight into a modified Finnigan MAT 90 fully laminated, double-focusing magnetic spectrometer. We have preserved the operation of the RF quadrupole principally as a backup when the magnetic spectrometer is inoperable for repairs or modification. The switch-yard also provides versatility if we need to insert new elements into the instrument, such as a charge neutralization system. The magnetic spectrometer is fitted with both a pulse-counting channeltron (for low signal detection) and a multistage dynode electron multiplier (for intense signals). The SIMS signals are routed to an image processor for post-

analysis. First results with this upgraded instrument demonstrate a sensitivity improvement of better than a factor of 40 for both positive and negative secondary ions. This value is obtained with a mass resolution of $m/\Delta m = 550$, 10% valley definition (to be compared with $m/\Delta m \approx 250$ FWHM typically derived from the previous RF quadrupole filter). Test mass spectra have been obtained with mass resolution ≈ 3500.

Acknowledgments

This work was funded by National Science Foundation under grants DMR 9015868 and 9111839, and by the Materials Research Laboratory at the University of Chicago. We would like to thank our collaborators D.B. Williams (Lehigh University), and V.P. Dravid and J. Hwang (Northwestern University) for providing samples and for constructive discussions. We are grateful to ILFORD Ltd. and ILFORD AG for supporting the research on photographic materials, and for providing the photographic samples.

Appendix 1

Listed below are selected recent articles describing applications of the University of Chicago scanning ion microprobe in the characterization of materials.

General reviews	Chabala *et al.* (1988b; 1989a; 1992), Levi-Setti *et al.* (1988a, 1988b, 1991).
Metallic materials	
Al-Li base alloys	Chabala *et al.* (1991), Soni *et al.* (1992b; 1993a), Williams *et al.* (1989).
Ceramics	
Sintered alumina	Soni *et al.* (1992d).
ZnO Varistors	Soni *et al.* (1992c).
Silicon nitride	Chabala *et al.* (1987).
Superconductors	Wang *et al.* (1989a), Chabala *et al.* (1989b), Levi-Setti *et al.* (1992).
Composites	
Metal- and Ceramic-matrix	Soni *et al.* (1993b), Williams *et al.* (1993).
Electronic Materials	
Integrated circuits	Chabala *et al.* (1988a), Levi-Setti *et al.* (1989).
Oxidation	
Solid state	Soni *et al.* (1991, 1992a).
Liquid state (*in-situ*)	Wang *et al.* (1989b), Chabala (1992).
Miscellaneous	
Photographic materials	Maternaghan *et al.* (1990).
Catalysts	Lampert *et al.* (1992).

References

Benninghoven A, Rüdenauer FG, Werner HW (1987). Secondary Ion Mass Spectrometry. Wiley, New York.

Chabala JM (1992). Oxide growth kinetics and fractal-like patterning across liquid gallium surfaces. Phys Res. **B46**, 11346-11357.

Chabala JM, Levi-Setti R, Bradley SA, Karasek K (1987). Imaging microanalysis of silicon nitride ceramics with a high resolution scanning ion microprobe. Appl. Surf. Sci. **29**, 300-316.

Chabala JM, Levi-Setti R, Wang YL (1988a). Imaging microanalysis of surfaces with a focused gallium probe. J. Vac. Sci. Technol. **B6**, 910-914.

Chabala JM, Levi-Setti R, Wang YL (1988b). Practical resolution limits of imaging microanalysis with a scanning ion microprobe. Appl. Surf. Sci. **32**, 10-32.

Chabala JM, Levi-Setti R, Wang YL (1989a). Advanced imaging and analysis techniques with a scanning ion microprobe. In: Microbeam Analysis-1989. San Francisco Press, San Francisco. 586-590.

Chabala JM, Chang RPR, Ketterson JB, Levi-Setti R, Li DX, Wang YL, Wang XK (1989b). Ion microprobe characterization of E-beam deposited YBaCu(F)O films: Effects of post-deposition processing. Physica C **162-164**, 75-76.

Chabala JM, Levi-Setti R, Soni KK, Williams DB, Newbury DE (1991). Secondary ion imaging of the distribution of $\delta'(Al_3Li)$ precipitates in binary Al-Li alloys. Appl. Surf. Sci. **51**, 185-192.

Chabala JM, Levi-Setti R, Li J, Parker NW, Utlaut M (1992). Development of a magnetic sector-based high lateral resolution scanning ion microprobe. In: SIMS-VIII. Benninghoven A, Janssen KTF, Tümpner J, Werner HW (eds.). Wiley, New York. 179-182.

Dhingra AK, Fishman SC (eds.) (1986). Interfaces in Metal Matrix Composites. The Metallurgical Society-AIME, Warrendale, PA, USA.

Gao XL, Jacob W, Gijbels R, Gilliams Y (1989a). Quantitative determination of the iodide content and distribution in different preparations of single tabular silver iodobromide microcrystals by scanning transmission electron microscopy with energy-dispersive X-ray spectrometry (STEM-EDX). In: Proc. SPSE 42nd Annual Conf. Available from: IS&T, The Society for Imaging Science and Technology, Springfield, VA. 34-35.

Gao XL, Nij B, Gijbels R, Gilliams Y, Jacob W (1989b). A new and convenient method for the analysis of the halide distribution in tabular silver halide microcrystals by backscattered electron imaging. In: Proc. SPSE 42nd Annual Conf. Available from: IS&T, The Society for Imaging Science and Technology, Springfield, VA. 31-33.

Geuens I, Gijbels R, Jacob W, Verbeeck A, DeKeyzer R (1992a). Analysis of silver halide microcrystals using different modes of a scanning transmission electron microscope and digital image processing. J. Imaging Sci. Technol. **36**, 534-539.

Geuens I, Gijbels R, Jacob W (1992b). Depth profiling of silver halide microcrystals. In: SIMS-VIII. Benninghoven A, Janssen KTF, Tümpner J, Werner HW (eds.). Wiley, New York. 479-482.

Geuens I, Gijbels R, Jacob W (1993). The Chemical characterization of silver halide microcrystals. In: Proc. IS&T 46nd Annual Conf. The Society for Imaging Science and Technology, Springfield, VA. 251-255.

Gupta TK (1990). Application of zinc oxide varistor. J. Am. Cer. Soc. **73**, 1817-1840.

Gupta TK, Miller AC (1988). Improved stability of the ZnO varistor via donor and acceptor doping at the grain boundary. J. Mater. Res. **3**, 745-754.

Keyes MP, Phillips EC, Gladfelter WL (1992). In situ atomic force microscopy of AgBr tabular grains: Surface effects of iodide. J. Imaging Sci. Technol. **36**, 268-272.

Lampert JK, Koermer GS, Macaoay JM, Chabala JM, Levi-Setti R (1992). Fluid catalytic cracking catalyst microstructure as determined by a scanning ion microprobe. Appl. Surf. Sci. **55**, 149-158.

Levi-Setti R, Chabala JM, Wang YL (1988a). Aspects of high resolution imaging with a scanning ion microprobe. Ultramicrosc **24**, 97-114.

Levi-Setti R, Chabala JM, Wang YL, Hallegot P (1988b). High resolution ion probe imaging and analysis. In: Microbeam Analysis-1988. San Francisco Press, San Francisco. 93-102.

Levi-Setti R, Chabala JM, Hallegot P, Wang YL (1989). Chemical characterization of electronic microstructures with sub-100 nm lateral resolution. Microelectronic Engr. **9**, 391-399.

Levi-Setti R, Hallegot P, Girod C, Chabala JM, Li J, Sodonis A, Wolbach WS (1991). Critical issues in the application of a gallium probe to high resolution secondary ion imaging. Surf. Sci. **246**, 94-106.

Levi-Setti R, Chabala JM, Sodonis AA, Seidler GT, Zhang K, Wolbach WS (1992). Anomalous secondary Cu^- ion yields in YBaCuO compounds. In: SIMS-VIII. Benninghoven A, Janssen KTF, Tümpner J, Werner HW (eds.). Wiley, New York. 769-772.

Maternaghan TJ, Falder CJ, Levi-Setti R, Chabala JM (1990). Elemental mapping of silver halide emulsion microcrystals by high resolution imaging SIMS. J. Imag. Sci. **34**, 58-65.

Sanders TH, Starke EA (1989). In: Proc. 5th Inter. Aluminum-Lithium Conf., Williamsburg, VA. M.A.C.E. Publications, Birmingham, U.K.

Soni KK, Williams DB, Chabala JM, Levi-Setti R, Newbury DE (1991). Morphological phenomena in the high temperature oxidation of binary Al-Li alloys. Oxid. Met. **36**, 361-378.

Soni KK, Williams DB, Chabala JM, Levi-Setti R, Newbury DE (1992a). Role of second-phase particles in the oxidation of binary Al-Li alloys. Oxid. Met. **37**, 23-37.

Soni KK, Williams DB, Chabala JM, Levi-Setti R, Newbury DE (1992b). Electron and ion microscopy studies of second-phase particles in binary Al-Li alloys. Acta Metall. Mater. **40**, 663-671.

Soni KK, Hwang J, Dravid VP, Mason TO Levi-Setti R (1992c). Microchemistry of ZnO Varistors. In: Proc. Electron Microscopy Society of America. San Francisco Press, San Francisco. 1694-1695.

Soni KK, Thompson AM, Harmer MP, Williams DB, Chabala JM, Levi-Setti R (1992d). SIMS studies of Ca and Mg distributions in sintered Al_2O_3. In: Proc. Electron Microscopy Society of America. San Francisco Press, San Francisco. 1772-1773.

Soni KK, Chabala JM, Levi-Setti R, Williams DB, Newbury DE, Bright DS (1993a). Phase equilibria in the Al-Li-Cu system determined by secondary ion mass spectrometry. Microbeam Analysis **2**, 13-21.

Soni KK, Chabala JM, Mogilevsky R, Levi-Setti R, Tseng MW, Williams DB (1993b). Ion microprobe investigations of interfacial phenomena in composites. JOM (Journal of TMS-AIME) **45**, 29-33.

Steiger R, Aebischer J-N, Haselbach E (1991). Influence of iodide ions on the adsorption of a cyanine dye on cubic AgBr emulsion crystals. J. Imaging Sci. **35**, 1-14.

Verpoest I, Jones F (eds.) (1991). Interfacial Phenomena in Composite Materials '91. Butterworth, Stoneham, MA.

Wang YL, Levi-Setti R, Chabala JM, Venkatesan T, Wu XD, Inam A, Dutta B (1989a). Ion microprobe analysis of laser-deposited Y-Ba-Cu-thin film: Effects of anneal temperature. J. Mater. Res. **4**, 1087-1092.

Wang YL, Raval A, Levi-Setti R (1989b). Dendritic oxide growth on the surface of liquid gallium. Scanning Microsc. **3**, 731-737.

Williams DB, Levi-Setti R, Chabala JM, Wang YL, Newbury DE (1989). Microanalysis of precipitates in aluminum-lithium alloys with a scanning ion microprobe. Appl. Surf. Sci. **37**, 78-94.

Williams DB, Soni KK, Tseng MW, Chabala JM, Levi-Setti R (1993). Scanning ion microprobe analysis of composite materials. J. Microsc. **169**, 163-172.

Discussion with Reviewers

C.G. Pantano: In general, how much material removal is required to generate these images? In Figure 2, specifically, does the O and F intensity depend inversely on the material removal rate? If so, the O and F may be absorbates due to system background.

Authors: A $(40\ \mu m)^2$ map acquired from a scan of 524 seconds duration (the maximum that we use) will remove approximately 30 monolayers of material, this is definitely not static SIMS! The reader can derive this result from the parameters: current = 30 pA, sputtering yield = 5. This sizeable depth must be eroded because, for high spatial resolution, the signal must be partitioned into 512 x 512 or 1024 x 1024 pixels, over a million data points. The greater transmission efficiency of the magnetic spectrometer allows quicker mapping, with less concomitant surface damage. (Note: the monolayer surface measurement of the AgBr crystals, Fig. 6b, was

acquired in 26 seconds.)

All measurements are performed at a pressure of $\sim 5 \times 10^{-9}$ Torr. Clearly, the material removal can keep ahead of the gas adsorption onto the surface.

R. Gijbels: You discuss the study of the surface distribution of I^- on AgBr (Fig. 6b). How many atomic layers (or sample thickness) must be sputtered to obtain a "good" ion image? Is it possible, by making a number of successive scans, to obtain (localized) depth profiles of halides in the surface/subsurface of silver halides?

Authors: The calculation above is also relevant to this question. The field of view for Figure 6b is $(10\ \mu m)^2$, the probe current was reduced to 20 pA, and the image was accumulated in 26 seconds (Br^- and I^- were acquired simultaneously via mass peak switching). Therefore, we estimate that about 16 monolayers or 5 nm of material are removed, given a unit cell spacing of 0.58 nm for AgBr. These are only order-of-magnitude figures, because the sputtering yield is not well known. If it is true that I lies only as a monolayer covering, then the I^- map is a representation of the top surface distribution. For this example, subsequent scans give no I^-, indicating that there is no internal iodine. Is Figure 6b a good image? It is human nature to always desire something better. The low statistics, spotty appearance of the I^- distribution was the best that could be done with the RF quadrupole system: all of the limited amount of I was consumed (there was less than a monolayer of I). Repeating this experiment with the magnetic spectrometer should provide at least 40 times more useful yield.

For crystals that are grown with heterogeneous internal halide structures, for example core/shell crystals with a layer of AgIBr, it is possible to obtain good localized depth profiles, essentially three dimensional SIMS maps. Some results of this type are presented in Geuens *et al.* (1993).

C.G. Pantano: The sample preparation is obviously an issue in all cases. Please comment on how the effects of surface preparation, especially of the (internal) composite interfaces, are eliminated or accounted for.

Authors: Metallographic preparation of heterogeneous materials may introduce topography or surface relief at the interphase interfaces. This topography may complicate interpretation of contrast in the SIMS maps due to edge effects. Similar problems affect electron probe analyses of rough surfaces. However, the secondary ions for SIMS are collected normal to the sample surface in our SIM, minimizing shadowing artifacts: edge effects are more pronounced in topography images than in SIMS maps. Also, the specimens are polished with care to reduce surface relief at the interfaces. Occasionally, surface relief still exists after polishing, especially at the submicrometer level that we are exploring. Figure 4b is an example where thin Na features might be the result, in part, of surface topography. There is no systematic procedure to account for this ambiguity, unfortunately. It is often possible to find an element that is emitted uniformly across the surface roughness, indicating that for that surface, edge effects are not pronounced.

R. Gijbels: To what extent is the use of Ga^+ primary ions (as compared to O_2^+, Cs^+ ...) limiting the sensitivity (useful ion yield) of the measurement? For Li^+ and I^-, e.g. there is clearly no problem. Which elements cannot be measured so well?

Authors: This is an interesting and pertinent question that we are now in the process of investigating systematically, as part of our program to fully characterize the magnetic sector mass spectrometer system. Before this investigation is complete, and without reference to data from systems that employ primary ions with similar energy (40 keV) but of a different species, we can only provide some general observations. By comparing ion yields generated by Ga^+ from pristine and oxidized surfaces, we find an O-induced enhancement that typically ranges by a factor from 10 to 100: this is presumably the advantage gained by using an oxygen probe. The Ga implant tends to improve (positive and negative) secondary ion yields by an unpredictable amount. Common elements that are difficult to map at low concentration with a Ga^+ probe are B, Fe, Cu. Among negative secondary ions, As^- is notoriously difficult to detect following Ga^+ bombardment without auxiliary chemical enhancement, such as an evaporated overlayer of Cs.

On a positive note, we have several ongoing investigations of oxide structures in metals, ceramics, and composite materials: these studies would be disrupted by the use of an oxygen primary beam. Non-reactive primary ions are best suited for many fundamental studies of surface physics. We would welcome the development of an intense, focused Ar^+ or Xe^+ probe.